**Atmospheric
Chemistry
and Physics
Discussions**

Radiometer
measurements of
HNO_3

M. Toohey et al.

Balloon-borne radiometer measurement of Northern Hemisphere mid-latitude stratospheric HNO_3 profiles spanning 12 years

M. Toohey[1], B. M. Quine[2], K. Strong[1], P. F. Bernath[3,4], C. D. Boone[4], A. I. Jonsson[1], C. T. McElroy[6], K. A. Walker[1,4], and D. Wunch[1,5]

[1]Department of Physics, University of Toronto, Toronto, ON, M5S 1A7, Canada
[2]School of Engineering, York University, Toronto, ON, M3J 1P3, Canada
[3]Department of Chemistry, University of York, Heslington, York, YO10 5DD, UK
[4]Department of Chemistry, Waterloo University, Waterloo, ON, N2L 3G1, Canada
[5]California Institute of Technology, Pasadena, CA, 91125, USA
[6]Environment Canada, Downsview, ON, M3H 5T4, Canada

Correspondence to: M. Toohey (mtoohey@atmosp.physics.utoronto.ca)

Title Page

Abstract | Introduction

Conclusions | References

Tables | Figures

◄◄ | ►►

◄ | ►

Back | Close

Full Screen / Esc

Printer-friendly Version

Interactive Discussion

EGU

Abstract

Low-resolution atmospheric thermal emission spectra collected by balloon-borne radiometers over the time span of 1990–2002 are used to retrieve vertical profiles of HNO_3, CFC-11 and CFC-12 volume mixing ratios between approximately 10 and 35 km altitude. All of the data analyzed have been collected from launches from a Northern Hemisphere mid-latitude site, during late summer, when stratospheric dynamic variability is at a minimum. The retrieval technique incorporates detailed forward modeling of the instrument and the radiative properties of the atmosphere, and obtains a best fit between modeled and measured spectra through a combination of onion-peeling and global optimization steps. The retrieved HNO_3 profiles are consistent over the 12-year period, and are consistent with recent measurements by the Atmospheric Chemistry Experiment-Fourier transform spectrometer satellite instrument. This suggests that, to within the errors of the 1990 measurements, there has been no significant change in the HNO_3 summer mid-latitude profile.

1 Introduction

One of the central aims of the Middle Atmosphere Nitrogen TRend Assessment (MANTRA) mission is to evaluate observational evidence for changes in the components of stratospheric total reactive nitrogen (NO_y). Towards this aim, two emission radiometer instruments have played an important and unique role in MANTRA balloon campaigns, due largely to the substantial flight heritage of the instrument design. The instruments measure atmospheric thermal emission in the 8–14 µm (715–1250 cm^{-1}) range, measuring the spectral emission features of many trace gas species, including emission at 11.3– µm due to nitric acid (HNO_3).

HNO_3 was first detected in the stratosphere though the use of balloon-borne filter radiometer instruments by Murcray et al. (1968), who soon afterwards identified the 11.3– µm spectral band as ideal for the measurement of HNO_3 due to minimal inter-

ference by other gases (Murcray et al., 1973). Balloon measurements led to a greater understanding of the vertical, latitudinal, and seasonal distribution of HNO_3 (Murcray et al., 1975) and the partitioning of active nitrogen between HNO_3, NO_2 and NO (e.g. Evans et al., 1977; Evans et al., 1982). Subsequent measurements by space-based (see Santee et al., 2004, and references therein), and balloon-borne instruments have led to a wealth of retrieved HNO_3 profiles.

Unfortunately, deriving a picture of the long-term behaviour of HNO_3 using the historical archive of retrieved profiles is complicated by inconsistencies in the spectroscopic parameters used to retrieve profiles from radiance measurements. Laboratory measurements of the line intensities in the 11.3–µm band, in particular, have yielded results which differ by as much as 30% (Flaud et al., 2006). Retrieved volume mixing ratio (VMR) magnitudes have been seen to be directly proportional to scaling of the line intensities (e.g. Irion et al., 2002), thus it is fair to say that there exist systematic discrepancies between the various retrieved profiles, with magnitudes up to 30%.

Furthermore, modern computational resources have allowed the improvement of the algorithms used to retrieve trace gas profiles from radiance observations. The earliest retrievals were based upon an onion-peeling technique (e.g. Evans et al., 1976) which required smoothing of the raw data. Quine et al. (2005) have shown that the resulting profiles can be greatly affected by the somewhat arbitrary choice of smoothing parameters. Also, the ability of modern retrieval algorithms to perform global fits can also greatly improve results (Irion et al., 2002).

In this work, we have collected data recorded by emission radiometer instruments during three MANTRA balloon flights (1998, 2000, and 2002), and during two flights in 1990. All data was collected through launches from a northern mid-latitude site (Vanscoy, Saskatchewan, 52° N, 107° W) during late summer when dynamical variability is minimal (Wunch et al., 2005). By analyzing the data with a consistent retrieval algorithm and spectroscopic line intensities, we connect modern measurements of HNO_3 with historical ones, and in so doing, develop a semi-quantitative picture of long-term HNO_3 profile changes.

EGU

2 HNO$_3$ in a changing atmosphere

HNO$_3$ is the principal component of NO$_y$ in the lower stratosphere, where it acts as a reservoir for the active nitrogen species NO and NO$_2$ involved in catalytic ozone loss cycles.

Changes in the abundance of HNO$_3$ are related to changes in the abundance of NO$_y$ and its partitioning. The source of stratospheric NO$_y$ is the transport of N$_2$O from the troposphere. Tropospheric N$_2$O has steadily increased by 3% per decade due to anthropogenic activities. McLinden et al. (2001) estimate that this increase in N$_2$O should lead to a 2.3% per decade increase in NO$_y$, with the difference due to nonlinear NO$_y$ loss processes in the upper atmosphere. Meanwhile, the partitioning of NO$_y$ has been modified by the increase of stratospheric chlorine. Modelling studies by Prather et al. (1984) have shown that as stratospheric concentrations of inorganic chlorine increase, ClONO$_2$ becomes more important as a NO$_y$ reservoir, leading to possible declines in HNO$_3$. HNO$_3$ is also highly sensitive to stratospheric aerosol loading through the heterogeneous reaction:

$$N_2O_5 + H_2O \rightarrow HNO_3 + HNO_3, \tag{R1}$$

which converts N$_2$O$_5$ to HNO$_3$ in the presence of aerosols.

Long-term changes in HNO$_3$ have been studied by use of ground-based observations of total columns, and space based, vertically resolved HNO$_3$ profiles. In an analysis of data comprised of solar spectra recorded with a grating spectrometer in June 1951 and a set of observations obtained with a Fourier transform spectrometer between June 1986 and June 1990, all from the International Scientific Station of the Jungfraujoch in Swiss Alps, Rinsland et al. (1991) found no significant change in the June HNO$_3$ total column over this time span. Randel et al. (1999) report statistically significant decreases of order 2% per year in lower stratospheric, extra-tropical HNO$_3$ between 1993 and 1997 based on analysis of observations made by the Microwave Limb Sounder (MLS) on board the Upper Atmosphere Research Satellite (UARS). While

EGU

the trend analysis excluded from consideration the MLS data from 1991–1992 in an attempt to remove the effects of elevated aerosol loading due to the Mt. Pinatubo eruption of 1991, ground-based measurements of HNO_3 total columns, and model results indicate NO_y partitioning may have been significantly perturbed until 1996 (Rinsland et al., 2003). To the authors' knowledge, no study has yet addressed long-term changes in HNO_3, apart from those due to aerosol loading from Mt. Pinatubo, by comparing consistent measurements from before and after the eruption.

The detection of trends in data is dependent upon the variability of the measured quantity (Weatherhead et al., 1998). In order to better understand the variability to be expected in HNO_3 profiles, we have studied simulated fields from the Canadian Middle Atmosphere Model. CMAM is an extended version of the Canadian Centre for Climate Modeling and Analysis spectral General Circulation Model. The dynamical core and chemistry scheme are described by Beagley et al. (1997) and de Grandpré et al. (1997) respectively. The current version of the model is discussed by Eyring et al. (2006), while the model results shown here are from a transient run described by Eyring et al. (2007). Chemical species have been saved every 18 h. Monthly mean CMAM HNO_3, at the vertical level of peak VMR ($\sim$24 km) and the model gridpoint closest to Vanscoy, Saskatchewan, are shown in Fig. (1) for ten years of the transient run. The seasonal cycle is apparent in the model output, with maximum HNO_3 in winter, and minimum in summer. The 2σ monthly variability of the 18-hourly data is shown by the shaded region. The average standard deviation of August HNO_3 values is approximately 6% of the mean, while in winter the same metric is 16%. Summer measurements are therefore the most useful measurements for assessing long-term changes in HNO_3.

3 Instrument design and history

The emission radiometer instruments used in this study were originally designed and fabricated by the Canadian Atmospheric Environment Service (AES) in the early 1970's based on a design first developed by Pick and Houghton (1969). The main design fea-

tures include (see Quine et al., 2005, Fig. 2): a mechanical chopper at the entrance slit, a spectral band-pass filter, a mercury-cadmium-telluride detector, amplifying electronics, and an insulated liquid-nitrogen dewar surrounding the detector and optics, maintaining a temperature of approximately 77 K. The instrument design also includes a blackbody calibration flap that is automatically lowered to cover the field-of-view periodically. The flap, mounted externally to maintain a temperature above that of liquid nitrogen, has an embedded platinum resistance thermometer to provide temperature information necessary for performing in-flight radiometric calibration.

The radiometer measures the cumulative spectroscopic gas emission along an upward-looking slant path. Vertical atmospheric information is made available by mounting the instrument, typically with a 20° elevation angle, on a balloon platform, and taking measurements while the balloon ascends. At the beginning of the balloon ascent, the instrument views a slant path through the whole atmosphere, and the radiance measurements are at a maximum. As the instrument ascends, the atmosphere below the instrument is excluded from the slant path, and the collected radiance decreases. A radiosonde is flown with the instrument in order to measure temperature and pressure, from which altitude is deduced via the hydrostatic relation.

When first fabricated, these instruments were furnished with five discrete band-pass filters to sample sections of the HNO$_3$ emission band at 11.3– µm. Radiance estimates were derived from these band-pass measurements and a careful filter calibration. Later instrument designs replaced the discrete filters with circular variable filter (CVF) segments. With two segments mounted on a constantly turning wheel, the instruments are able to scan a wavelength region from 8–14 µm (715–1250 cm^{-1}) with a band-pass varying between 1% and 4% of the center wavelength. A number of these scanning emission radiometers were flown on a series of AES test flights from Vanscoy, Saskatchewan from 1989–1991 before being used in non-recovered Arctic flights. Two surviving instruments, code-named MX-31 and MX-36 were refurbished with minimal modifications and used in the biennial MANTRA flights of 1998–2004.

4 Retrieval

Vertical profiles of HNO_3 were originally retrieved from data measured by the emission radiometer instrument through an onion-peeling algorithm, wherein the amount of HNO_3 between two measurement altitudes was assumed to be proportional to the change in radiance between the measurements (Evans et al., 1976). Instrument parameters were determined through pre- and post-flight calibration.

Quine et al. (2005) introduced an updated retrieval algorithm for the emission radiometer, based on detailed forward modelling of the atmosphere and instrument. Given atmospheric temperature and pressure information, expected trace gas abundances, and some instrument calibration parameters, these models simulate the spectral scans recorded by the instrument during flight. An optimization routine is used to obtain a best fit between the simulated and measured spectra by adjusting the instrument parameters and trace gas amounts. The main advantage of this technique is the incorporation of instrument parameters into the retrieved state vector, which allows the analysis of flight data without pre- and post- calibration data. We summarize the main points of the retrieval algorithm below, with special emphasis on modifications made since the work of Quine et al. (2005).

4.1 Atmospheric forward model

The atmosphere is modelled as a set of discrete 2-km-thick cells on a vertical grid. For each cell, a density-weighted effective mean temperature and pressure are determined using the Curtis-Godson approximation (Houghton, 1986), based on sonde measurements. Spectral absorption coefficients for each cell and for eight principal emitting gas species (H_2O, CO_2, O_3, N_2O, CH_4, HNO_3, CFC-11 and CFC-12) are calculated using the GENSPECT line-by-line code (Quine and Drummond, 2002) with HITRAN 2004 data (Rothman et al., 2005). HITRAN line parameter updates for HNO_3 are included (Flaud et al., 2006), based on work that went into the MIPAS (Michelson Interferometer for Passive Atmospheric Sounding) database. Radiative transfer code included in the

EGU

GENSPECT package is used to calculate the radiance at each cell boundary based on the blackbody emission and transmission of each cell. This simulated spectral radiance profile is linearly interpolated to the radiometer measurement heights, and passed as the main input into the instrument forward model.

4.2 Instrument forward model

The aim of the instrument forward model is to accurately simulate the true mapping between input radiance and detector response. While it is assumed that the individual instruments are for the most part functionally identical, a few instrument parameters defining unique properties of the instruments are necessary, and are included in the forward model.

Two parameters define the mapping between CVF angular position and wavenumber. A linear relationship between CVF position and wavelength is reported by the CVF manufacturer and assumed here. Initial estimates for the two parameters are produced manually by finding the angular position of the O_3 and HNO_3 peaks in the raw data. These instrument parameters are then included in the retrieval, and serve to shift and stretch the data in order to match the simulated spectra.

A third instrument parameter is used in the construction of the instruments' slit function. The shape of the slit function, and the relationship between width and center wavelength is based upon Fourier transform spectrometer measurements of the band-pass of a sample CVF. A retrieved instrument parameter specifies the width of a boxcar function convolved with this experimental slit function, accounting for the finite angular width of the focussed light passing through the CVF in each particular instrument.

The instrument is modelled so as to assume a relationship between detector response S at a given wavenumber v' and incident radiance spectrum I for a given effective viewing angle $\hat{\theta}$ as follows:

$$S(v', z) = R(v', z) \int_0^\infty I(v, \hat{\theta}, z) F(v - v') dv + \varepsilon \tag{1}$$

where R is the instrument responsivity as a function of altitude, F is the slit function, and ε is a dark current level.

Dark current noise is defined for each scan by the average signal measured as an opaque section of the CVF attenuates the input radiation.

The effective viewing angle $\hat{\theta}$ is an approximate quantity describing the mean elevation angle of light collected by the instrument. It is a function of the mounting angle of the instrument on the balloon payload, the field-of-view (FOV) function of the instrument describing the angular dependence of the instrument's ability to collect radiation, and the radiation field as a function of angle. In order to define a constant $\hat{\theta}$ for any measurement set, we assume a plane parallel atmosphere with homogeneous emission. The radiation field is then given by the cosecant function describing the variation of atmospheric slant path with elevation angle, and $\hat{\theta}$ is given by the mean of the product of the FOV and cosecant functions. The FOV, as determined by laboratory tests, is roughly toroidal, with sensitivity extending to ±16° and maximum sensitivity at ±9°. The effective viewing angle for an instrument mounted at 20° elevation angle is approximately 17°.

In-flight blackbody calibration scans, performed every fifth scan at altitudes z', are used to define instrument responsivity function R. The responsivity of the instrument changes as a function of altitude, due to changes in atmospheric pressure and temperature. The responsivity function is calculated as the ratio of detector output S (with dark current ε subtracted) to the theoretical blackbody radiance curve (based on the temperature measured by the flap thermometer) convolved by the instrument slit function:

$$R(v', z') = \frac{S(v', z') - \varepsilon}{\int_0^\infty B_v(v, T) F(v - v') dv}. \tag{2}$$

The responsivity function is then interpolated to the atmospheric measurement heights (z) in order to calculate the simulated spectra via Eq. (1).

4.3 Optimization

The objective function is defined as the sum of squares of the difference between the simulated and measured spectral scans. The optimal retrieval is that which minimizes this objective function.

Prior work (Quine et al., 2005) introduced the use of a non-linear global optimization algorithm used to search for a global minimum by iteratively perturbing the full state vector of instrument parameters and trace gas species on the full vertical grid. While this technique produced reasonable results, it required large amounts of computing resources, and time. In order to produce results on a faster time scale we have modified this approach.

In the latest approach, a first stage retrieval defines a state vector of instrument parameters and scale factors which multiply a priori trace gas profiles. The objective function to be minimized is based solely on spectral scans within the lowermost atmospheric cell. These low-altitude scans provide the most information regarding the instrument parameters, since they contain significant radiance contributions from HNO_3, CFC-11 and CFC-12. The Direct global optimization routine (Jones et al., 1993) is used.

A second stage performs onion-peeling while keeping the instrument parameters fixed. Starting at the uppermost atmospheric cell and moving down, trace gas amounts are adjusted in order to minimize the measurement residual within that cell in the local spectral neighbourhood of the emission peak for each of the three species. The onion-peeling proceeds by the method of steepest descent, with the local gradient defined by first perturbing the cell VMR by 1%, and using the forward model to calculate the corresponding change in radiance. This process is repeated iteratively until the difference between the measured and simulated radiances reaches a preset convergence criterion. Weighting functions and averaging kernels for the onion-peeling algorithm are given in Quine et al. (2005).

The global fit – onion-peeling sequence outlined above is then repeated, with the only

difference being that the global optimization in step one is performed with the objective function defined using scans over the full altitude range. Comparison of simulated and measured spectral scans for a sample instrument and year are shown in Fig. (2).

4.4 Error analysis

Within the final onion peeling step of the retrieval, a root-mean-square (RMS) residual is calculated between the simulated and measured spectra in the neighbourhood of the emission peak for each gas species fit. This RMS is divided by the local change in radiance for a given change in trace gas VMR in order to estimate the retrieval error based on radiance noise.

The recorded temperature of the blackbody flaps is another major source of uncertainty. Laboratory tests have produced calibration coefficients for the two instruments used in MANTRA flights. Based on these tests, we conservatively estimate the temperature error of the MANTRA blackbody flaps as 2 K. Corresponding VMR errors have been calculated by simply performing the retrieval on raw data perturbed by the temperature uncertainty estimate. A 2 K error in temperature leads to a HNO_3 VMR error of approximately 10% at 24 km.

Lastly, the uncertainty in the effective elevation angle is estimated to be $\pm 0.5°$, which corresponds to an error of approximately 2.5% at 24 km.

Radiance error, blackbody temperature error, and viewing angle error are added in quadrature to obtain the total error as a function of altitude.

5 Data

Each MANTRA mission has included on the instrument payload two radiometers, MX-31 and MX-36. The two instruments were mounted with different elevation angles, with one at 20° and the other at 30–40°. Raw data of good quality was collected by both instruments during the flights of 1998 and 2000. One instrument failed in

2002, and both instruments failed in 2004, likely due to the effect of ice build-up on the mechanically rotating CVF.

The AES test flights of 1990 suffered from a variety of fatal and non-fatal failures, making the raw data difficult to process. All flights suffered from poor data quality due to transponder drop-outs. Many flights also suffered from obvious mis-calibration of the blackbody flap temperatures.

We include in this work results from two radiometer flights of August 1990. Of all data from the AES test flights, that from MX-19 on 30 August is of the highest quality. The ubiquitous transponder drop-outs and a higher-than-expected spectral noise are the data's only significant faults. Data from MX-13, flown on 20 August 1990, suffered some more critical non-fatal effects. Time synchronization between the radiometer clock and the radiosonde clock (in order to achieve proper altitude registration) was produced by defining a time offset that minimized the residual between the time derivatives of the sonde-measured air temperature and the instrument flap temperature. Furthermore, the flap temperature was bias corrected in order to bring the difference between flap temperature and air temperature into a range comparable to the other flights. Due to these necessary pre-processing steps, we have estimated the temperature error of the blackbody flaps for this flight at 5 K.

We will compare our retrieved profiles of HNO_3, CFC-11 and CFC-12 with results from the Atmospheric Chemistry Experiment – Fourier transform spectrometer (hereinafter ACE) satellite instrument, launched in August 2003. We compare with ACE since it simultaneously retrieves all three species measured by the radiometers, and since ACE data has previously been used in a trend analysis of many species, including CFC-11 and CFC-12 (Rinsland et al., 2005). ACE is a Fourier transform spectrometer operating at high spectral resolution in the infrared, measuring atmospheric extinction by solar occultation, from which profiles of temperature, pressure and dozens of constituents are retrieved through a global fitting algorithm (Bernath et al., 2005; Boone et al., 2005). ACE results are from the version 2.2 data set. HNO_3 retrievals from ACE employ a set of microwindows near 900 cm^{-1} (11.3– µm), and another set near

EGU

1700 cm^{-1}, and use the HITRAN 2004 spectral database. ACE retrievals do not use the Flaud et al. (2006) HNO$_3$ update, but the impact of the update to HITRAN 2004 in the 11.3–µm spectral range is small: the percent change in integrated line intensity over this band is on the order of 2% (Flaud et al., 2006). ACE retrievals have

5 been shown to have good (relative differences of 5–10% below 30 km) agreement with MIPAS operational retrievals (Wang et al., 2007a), and the MIPAS IMK-IAA research product (Wang et al., 2007b). Due to the orbit and solar occultation technique used by the ACE platform, the latitudinal distribution of measurements is highly dependant upon the time of year. ACE samples the Northern mid-latitudes in late summer briefly

10 at the beginning of September (see Fig. 3), in close proximity to the window of past MANTRA flights (24 August–3 September). For the comparison, we take averages of these late summer ACE measurements from 2004–2006 over the 10° latitude band centered on the latitude of Vanscoy, Saskatchewan.

6   Results

15 The retrieved profiles of HNO$_3$ are shown in Fig. (4). The mean profile for the MANTRA missions (1998–2002) is shown on each panel for comparison. The retrieved profiles are remarkably consistent. The two retrieved profiles for the flights with simultaneous measurements (1998 and 2000) are equivalent at almost all altitudes. Small differences between the simultaneous measurements are likely due to differences in hori-

20 zontal sampling by the two instruments mounted with differing elevation angles, and the local horizontal gradient in the HNO$_3$ field. The error in the 1990 profiles is large, due to uncertainties in the blackbody flap temperature and the measured radiance noise. Despite this, the profiles are not inconsistent with the MANTRA mean profile.

The MANTRA-mean profiles of HNO$_3$, CFC-11 and CFC-12 are compared to mean

25 Northern Hemisphere mid-latitude late summer retrieved profiles from the ACE satellite instrument in Fig. (5). The comparison shows excellent agreement for HNO$_3$: the MANTRA-mean HNO$_3$ profiles lie within the ACE 2σ variability for all but the very high-

est altitudes. CFC profiles retrieved from the radiometers exibit a larger degree of scatter and inter-instrument bias, as shown by the 1σ error bars. The individual retrieved profiles have errors between 20 and 100% between 12 and 24 km (not shown). Despite this, the mean radiometer CFC profiles are comparable in shape to the ACE measurements, although somewhat larger in magnitude. In a comparison of measurements by the Atmospheric Trace Molecule Spectroscopy Experiment (ATMOS) in 1985 and 1994 and by ACE in 2004, Rinsland et al. (2005) find very little difference between CFC-11 and CFC-12 stratospheric mixing ratios between 1994 and 2004. Given this result, we suggest the differences between ACE and MANTRA-mean CFC profiles are due to the large random error in the MANTRA radiometer measurements and the small sample size.

Are the MANTRA HNO_3 measurements consistent with the variability of the CMAM? Figure (6) addresses this question by plotting the percent standard deviation of the MANTRA retrieved profiles and that from the 18-hourly data from the final week of August over 10 CMAM years. The two profiles show similar structure, with larger values in the lower stratosphere, and a broad minimum between 20 and 30 km. This comparison is somewhat unfair as the MANTRA HNO_3 measurements represent a very sparse sampling of the true HNO_3 late-summer time series, with only three independent samples. We address the issue of sparse sampling by MANTRA by calculating the standard deviation of the model profiles using only three random samples. By iterating this procedure a large number of times, we produce a probability distribution function of the calculated standard deviation for the given MANTRA sampling, and define a 99% confidence interval, shown in grey shading in Fig. (6). By repeating the same procedure, but adding a 10% random error onto the sampled CMAM profiles, we get an even better sense of the variability expected in the MANTRA measurements. Between 15 and 30 km height, the variability of the MANTRA measurements is seen to be consistent with the variability of the model, given the sparsity and uncertainty of the measurements. Above 30 km and below 15 km, the variance of the MANTRA measurements is apparently adversely affected by instrument error.

The variance of ACE HNO_3 measurements is in excellent agreement with that of the CMAM (Fig. 6). On the one hand, this close agreement validates our use of the model to explore the sampling issues inherent in the MANTRA measurements. On the other hand, under the assumption that the CMAM gives a good estimate of the variability of the true atmosphere, any difference between the CMAM and ACE variances should be due to the random error of the ACE retrievals. The close agreement between the measured and modelled variance is then evidence that ACE measurements display a high degree of precision.

7 Conclusions

We have analyzed raw data recorded by low-resolution scanning infrared radiometers from balloon flights in 1990, 1998, 2000, and 2002, and retrieved vertical profiles of HNO_3 using current spectroscopic line parameters and an efficient retrieval technique making use of both global-fitting and onion-peeling routines. The retrieved HNO_3 profiles show excellent agreement, in profile shape and magnitude, with measurements made by the ACE satellite instrument at a similar season and latitude region over the years 2004–2006. The measurements were taken over a mid-latitude Northern Hemisphere site in late summer, when stratospheric dynamical and chemical variability is minimal. The variance of the HNO_3 profiles measured over the MANTRA era (1998–2002) is in good agreement with the variability estimated by the CMAM, when the limited sampling and error of the measurements are taken into account. The radiometer measurements represent a consistent data set with samples before and after the Mt. Pinatubo eruption. While the error on the measurements from 1990 is large, and the data set is small, we see no significant change in the vertical profile of HNO_3 over this time span. This result may be taken as direct evidence that the –2% per year HNO_3 trend measured by the UARS-MLS instrument over the time span 1993–1997 (Randel et al., 1999) represents a slow relaxation of the NO_y partitioning from the perturbed conditions after the Mt. Pinatubo eruption of 1991, as is suggested by the modelling

component of work by Rinsland et al. (2003), rather than any underlying long-term trend.

References

Beagley, S. R., de Grandpré, J., Koshyk, J. N., McFarlane, N. A., and Shepherd, T. G.: Radiative-dynamical climatology of the first-generation Canadian Middle Atmosphere Model, Atmos. Ocean, 35, 293–331, 1997. 11565
Bernath, P. F., McElroy, C. T., Abrams, M. C., Boone, C. D., Butler, M., Camy-Peyret, C., Carleer, M., Clerbaux, C., Coheur, P.-F., Colin, R., DeCola, P., DeMazière, M., Drummond, J. R., Dufour, D., Evans, W. F.J., Fast, H., Fussen, D., Gilbert, K., Jennings, D. E., Llewellyn, E. J., Lowe, R. P., Mahieu, E., McConnell, J. C., McHugh, M., McLeod, S. D., Michaud, R., Midwinter, C., Nassar, R., Nichitiu, F., Nowlan, C., Rinsland, C. P., Rochon, Y. J., Rowlands, N., Semeniuk, K., Simon, P., Skelton, R., Sloan, J. J., Soucy, M.-A., Strong, K., Tremblay, P., Turnbull, D., Walker, K. A., Walkty, I., Wardle, D. A., Wehrle, V., Zander, R., and Zou, J.: Atmospheric Chemistry Experiment (ACE): Mission overview, Geophys. Res. Lett., 32, L15S01, doi:10.1029/2005GL022386, 2005. 11572
Boone, C. D., Nassar, R., Walker, K. A., Rochon, Y., McLeod, S. D., Rinsland, C. P., and Bernath, P. F.: Retrievals for the atmospheric chemistry experiment Fourier-transform spec-trometer, Appl. Optics, 44, 7218–7231, 2005. 11572
de Grandpré, J., Sandilands, J. W., McConnell, J. C., Beagley, S. R., Croteau, P. C., and Danilin, M. Y.: Canadian Middle Atmosphere Model: Preliminary results from the chemical transport module, Atmos. Ocean, 35, 385–431, 1997. 11565

Radiometer measurements of HNO$_3$

M. Toohey et al.

Title Page

Abstract	Introduction
Conclusions	References
Tables	Figures

◄◄   ►►

◄   ►

Back   Close

Full Screen / Esc

Printer-friendly Version

Interactive Discussion

EGU

Evans, W. F. J., Lin, C. I., and Midwinter, C. L.: The Altitude Distribution of Nitric Acid at Churchill, Atmosphere, 14, 172–179, 1976. 11563, 11567

Evans, W. F. J., Kerr, J. B., McElroy, C. T., Obrien, R. S., Wardle, D. I., and Ridley, B. A.: The odd nitrogen mixing ratio in the stratosphere, Geophys. Res. Lett., 4, 235–238, 1977. 11563

Evans, W. F. J., Kerr, J. V., McElroy, C. T., O'Brien, R. S., and McConnell, J. C.: Measurements of NO_2 and HNO_3 during a stratospheric warming at 54 in February 1979, Geophys. Res. Lett., 9, 493–496, 1982. 11563

Eyring, V., Waugh, D. W., Bodeker, G. E., Cordero, E., Akiyoshi, H., Austin, J., Beagley, S. R., Boville, B., Braesicke, P., Brühl, C., Butchart, N., Chipperfield, M. P., Dameris, M., Deckert, R., Deushi, M., Frith, S. M., Garcia, R. R., Gettelman, A., Giorgetta, M., Kinnison, D. E., Mancini, E., Manzini, E., Marsh, D. R., Matthes, S., Nagashima, T., Newman, P. A., Nielsen, J. E., Pawson, S., Pitari, G., Plummer, D. A., Rozanov, E., Schraner, M., Scinocca, J. F., Semeniuk, K., Shepherd, T. G., Shibata, K., Steil, B., Stolarski, R., Tian, W., and Yoshiki, M.: Multi-model projections of stratospheric ozone in the 21st century, J. Geophys. Res., in press, 2007. 11565

Eyring, V., Butchart, N., Waugh, D. W., Akiyoshi, H., Austin, J., Bekki, S., Bodeker, G. E., Boville, B. A., Brühl, C., Chipperfield, M. P., et al.: Assessment of temperature, trace species, and ozone in chemistry-climate model simulations of the recent past, J. Geophys. Res., 111, D22308, doi:10.1029/2006JD007327, 2006. 11565

Flaud, J.-M., Brizzi, G., Carlotti, M., Perrin, A., and Ridolfi, M.: MIPAS database: Validation of HNO_3 line parameters using MIPAS satellite measurements, Atmos. Chem. Phys., 6, 5037–5048, 2006,
http://www.atmos-chem-phys.net/6/5037/2006/. 11563, 11567, 11573

Houghton, J. T.: The Physics of Atmospheres, Cambridge University Press, 45pp., 1986. 11567

Irion, F. W., Gunson, M. R., Toon, G. C., Chang, A. Y., Eldering, A., Mahieu, E., Manney, G. L., Michelsen, H. A., Moyer, E. J., Newchurch, M. J., et al.: Atmospheric Trace Molecule Spectroscopy (ATMOS) Experiment Version 3 data retrievals, Appl. Optics, 41, 6968–6979, 2002. 11563

Jones, D. R., Perttunen, C. D., and Stuckman, B. E.: Lipschitzian optimization without the Lipschitz constant, J. Optimiz. Theory App., 79, 157–181, 1993. 11570

McLinden, C. A., Olsen, S. C., Prather, M. J., and Liley, J. B.: Understanding trends in stratospheric NO_y and NO_2, J. Geophys. Res., 106, 27 787–27 793, 2001. 11564

Murcray, D. G., Kyle, T. G., Murcray, F. H., and Williams, W. J.: Nitric acid and nitric oxide in the

Title Page

Abstract | Introduction

Conclusions | References

Tables | Figures

◄◄ | ►►

◄ | ►

Back | Close

Full Screen / Esc

Printer-friendly Version

Interactive Discussion

EGU

lower stratosphere, Nature, 218, 78–79, 1968. 11562

Murcray, D. G., Goldman, A., Csoeke-Poeckh, A., Murcray, F. H., Williams, W. J., and Stocker, R. N.: Nitric acid distribution in the stratosphere, J. Geophys. Res., 78, 7033–7038, 1973. 11563

5 Murcray, D. G., Barker, D. B., Brooks, J. N., Goldman, A., and Williams, W. J.: Seasonal and latitudinal variation of the stratospheric concentration of HNO_3, Geophys. Res. Lett., 2, 223–225, 1975. 11563

Pick, D. R. and Houghton, J. T.: Measurements of atmospheric infrared emission with a balloon-borne multifilter radiometer, Q. J. Roy. Meteor. Soc., 95, 535, 1969. 11565

10 Prather, M. J., McElroy, M. B., and Wofsy, S. C.: Reductions in ozone at high concentrations of stratospheric halogens, Nature, 312, 227–231, 1984. 11564

Quine, B. M. and Drummond, J. R.: GENSPECT: A new generation line-by-line code with a bounded interpolation accuracy, J. Quant. Spectrosc. Ra., 74, 147–165, 2002. 11567

Quine, B. M., Toohey, M., Drummond, J. R., Strong, K., Wunch, D., Midwinter, C., and McElroy,
15 C. T.: The Concentration Profile of Nitric Acid and Other Species over Saskatchewan in August 1998: Retrieval from Data Recorded by Thermal-Emission Radiometry, Atmos. Ocean, 43, 361–376, 2005. 11563, 11566, 11567, 11570

Randel, W. J., Wu, F., Russel III, J. M., and Waters, J. W.: Space-time patterns of trends in stratospheric constituents derived from UARS measurements, J. Geophys. Res., 104(D3),
20 3711pp., 1999. 11564, 11575

Rinsland, C. P., Zander, R., and Demoulin, P.: Ground-based infrared measurements of HNO_3 total column abundances: long-term trend and variability, J. Geophys. Res., 96, 9379–9389, 1991. 11564

Rinsland, C. P., Weisenstein, D. K., Ko, M. K. W., Scott, C. J., Chiou, L. S., Mahieu, E., Zander,
25 R., and Demoulin, P.: Post-Mount Pinatubo eruption ground-based infrared stratospheric column measurements of HNO_3, NO and NO_2 and their comparison with model calculations, J. Geophys. Res., 108(D15), 4437, doi:10.1029/2002JD002965, 2003. 11565, 11576

Rinsland, C. P., Boone, C., Nassar, R., Walker, K., Bernath, P., Mahieu, E., Zander, R., McConnell, J. C., and Chiou, L.: Trends of HF, HCl, CCl_2F_2, CCl_3F, $CHClF_2$ (HCFC-22), and SF_6
30 in the lower stratosphere from Atmospheric Chemistry Experiment (ACE) and Atmospheric Trace Molecule Spectroscopy (ATMOS) measurements near 30° N latitude, Geophys. Res. Lett., 32, L16S03, doi:10.1029/2005GL022415, 2005.' 11572, 11574

Rothman, L. S., Jacquemart, D., Barbe, A., Chris Benner, D., Birk, M., Brown, L. R., Carleer,

M. R., Chackerian, C., Chance, K., Coudert, L. H., et al.: The HITRAN 2004 molecular spectroscopic database, J. Quant. Spectrosc. Ra., 96, 139–204, 2005. 11567

Santee, M. L., Manney, G. L., Livesey, N. J., and Read, W. G.: Three-dimensional structure and evolution of stratospheric HNO_3 based on UARS Microwave Limb Sounder measurements, J. Geophys. Res., 109, D15306, doi:10.1029/2004JD004578, 2004. 11563

Wang, D. Y., Höpfner, M., Blom, C. E., Ward, W. E., Fischer, H., Blumenstock, T., Hase, F., Keim, C., Liu, G. Y., Mikuteit, S., et al.: Validation of MIPAS HNO_3 operational data, Atmos. Chem. Phys. Discuss., 7, 5173–5251, 2007a. 11573

Wang, D. Y., Höpfner, M., Tsidu, G. M., Stiller, G. P., von Clarmann, T., Fischer, H., Blumen-stock, T., Glatthor, N., Grabowski, U., Hase, F., et al.: Validation of nitric acid retrieved by the IMK-IAA processor from MIPAS/ENVISAT measurements, Atmos. Chem. Phys., 7, 721–738, 2007b. 11573

Weatherhead, E. C., Reinsel, G. C., Cheang, W. K., Tiao, G. C., Meng, X. L., Choi, D., Keller, T., DeLuisi, J., Wuebbles, D. J., and Kerr, J. B.: Factors affecting the detection of trends-Statistical considerations and applications to environmental data, J. Geophys. Res., 103, 17–149, 1998. 11565

Wunch, D., Tingley, M. P., Shepherd, T. G., Drummond, J. R., Moore, G. W. K., and Strong, K.: Climatology and predictability of the late summer stratospheric zonal wind turnaround over Vanscoy, Saskatchewan, Atmos. Ocean, 43, 301–313, 2005. 11563

Title Page

Abstract | Introduction

Conclusions | References

Tables | Figures

◄◄ | ►►

◄ | ►

Back | Close

Full Screen / Esc

Printer-friendly Version

Interactive Discussion

EGU

EGU

Table 1. Balloon flights of the radiometer dataset.

| Flight	Date	Instruments
AES	Aug 20, 1990	MX13
AES	Aug 30, 1990	MX19
MANTRA	Aug 24, 1998	MX31, MX36
MANTRA	Aug 29, 2000	MX31, MX36
MANTRA	Sep 03, 2002	MX31

EGU
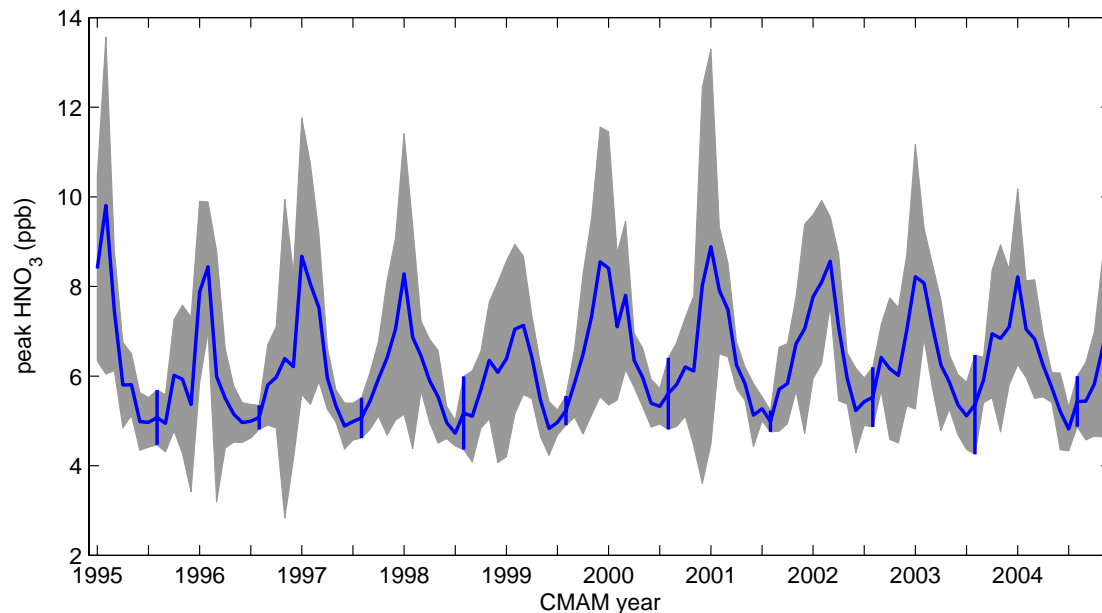
Fig. 1. Time series of monthly mean HNO₃ volume mixing ratio (VMR) at ∼24 km from the Canadian Middle Atmosphere Model (CMAM). Monthly variability (2σ) is represented by shading, and August variability values are highlighted by vertical lines.

EGU
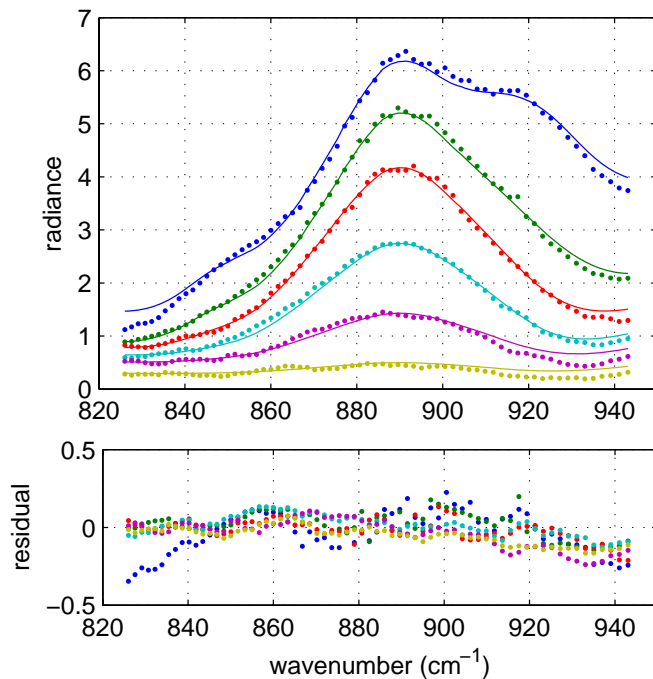
Fig. 2. An example selection of spectral fits and residuals, approximately equally spaced between 12 and 30 km height, from the emission radiometer fitting routine. Results shown are for MANTRA 2000, MX-36. Plotted points represent the measurement scans, while lines show the simulated spectra.

EGU
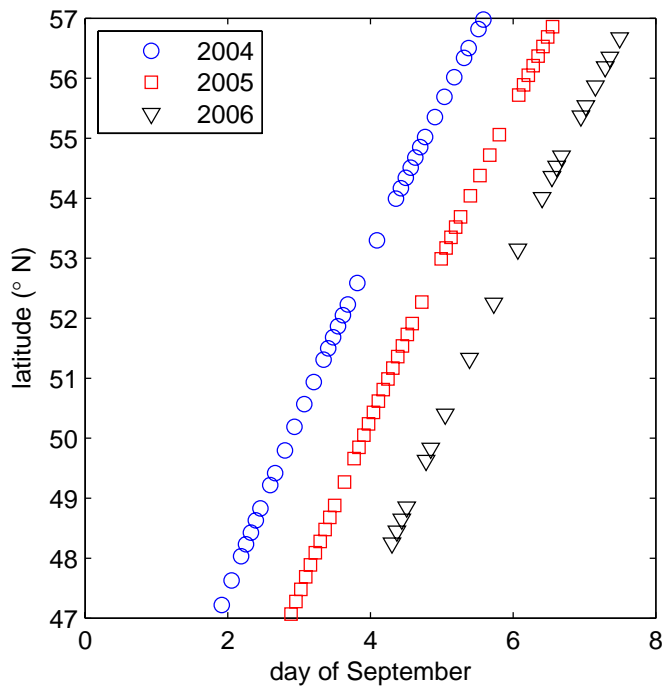
Fig. 3. Time-latitude coordinates of Northern Hemisphere mid-latitude ACE occultations in late summer, over three years.
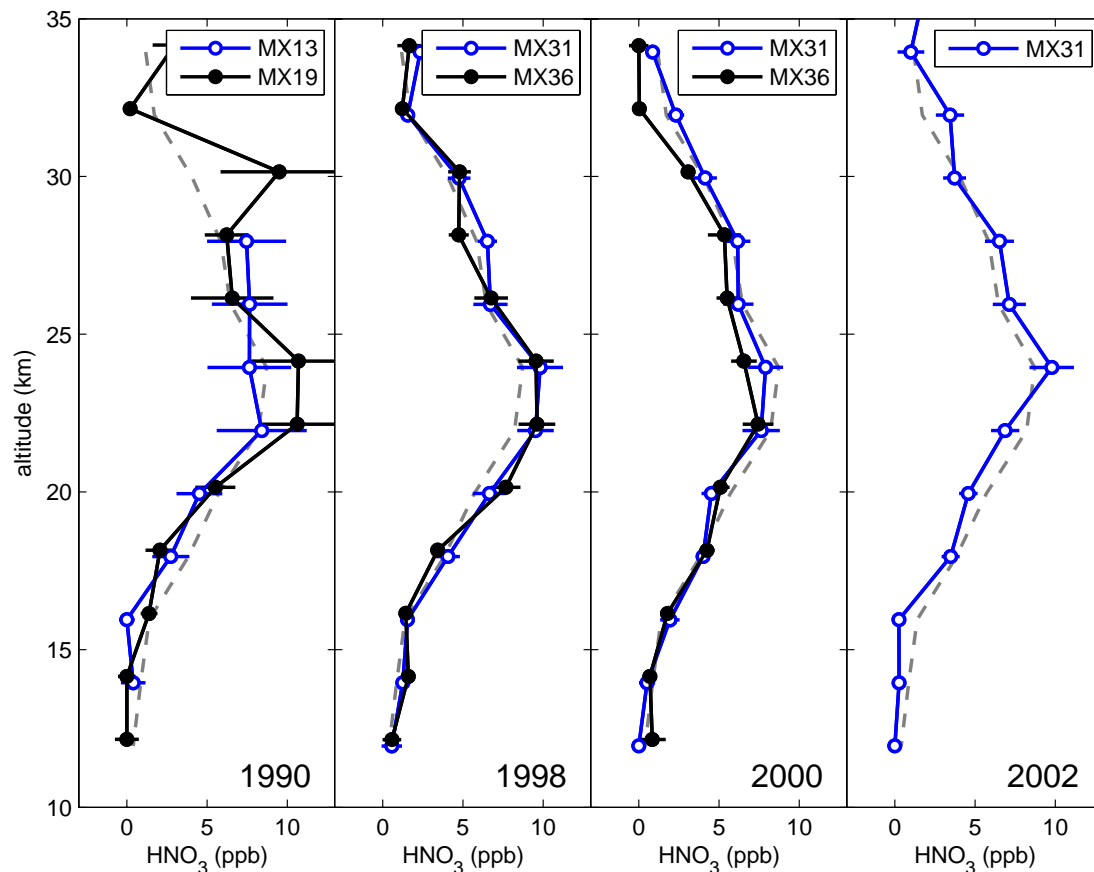
Fig. 4. Retrieved HNO$_3$ profiles for the years shown. Instrument code names, specifying the source of the radiance data used in each retrieval, are given in the legend (see Table 1). Error bars show the estimated uncertainty in the retrievals. The mean profile over MANTRA missions (1998–2002) is shown by the dashed line.

ACPD

7, 11561–11586, 2007

Radiometer measurements of HNO$_3$

M. Toohey et al.

Title Page

Abstract | Introduction

Conclusions | References

Tables | Figures

|◄ | ►|

◄ | ►

Back | Close

Full Screen / Esc

Printer-friendly Version

Interactive Discussion

EGU
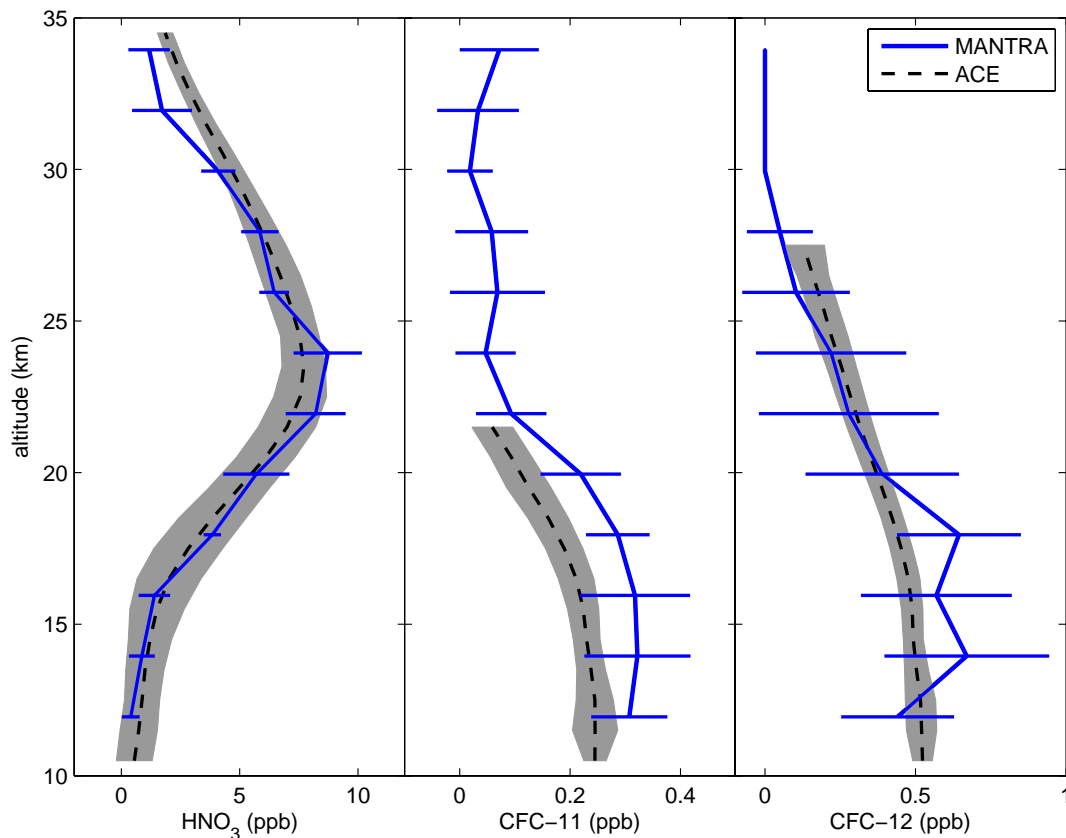
Fig. 5. Mean profiles of HNO$_3$, CFC-11 and CFC-12 VMR from the MANTRA flights (1998–2002) and from observations by the ACE satellite instrument (2004–2006). Shading represents the 2σ variability of the ACE profile, while the error bars on the MANTRA radiometer profiles represent 1σ variability in the retrieved profiles.

EGU
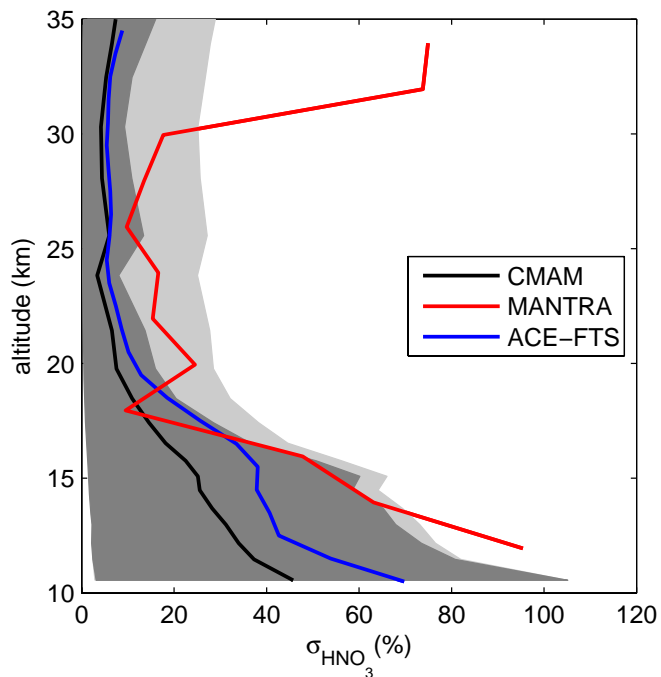
Fig. 6. Percent standard deviations of HNO$_3$ VMR profiles from ACE measurements, MANTRA measurements, and simulated fields from CMAM. Grey shading represents the 99% confidence interval of values given by CMAM when only three independent samples are used (dark grey), and with an added 10% error on each sample (light grey).